11th International Symposium on Turbulence and Shear Flow Phenomena (TSFP11)
Southampton, UK, July 30 to August 2, 2019

LARGE SCALE COHERENT STRUCTURES IN A ZPG TURBULENT BOUNDARY LAYER FOR THE MACH NUMBER RANGE 0.3 − 3.0

Matthew Bross, Sven Scharnowski and Christian J. Kähler
Institute of Fluid Mechanics and Aerodynamics
Universität der Bundeswehr München
Werner-Heisenberg-Weg 39,
85577 Neubiberg, Germany
Correspondent author: matthew.bross@unibw.de

Abstract

The presence of large scale coherent structures in various wall bounded turbulent flows, including turbulent boundary layers, has been of great interest in recent years. These meandering high- and low-momentum structures can extend up to several boundary layer thicknesses and contain a relatively large potion of the layer's turbulent kinetic energy. Therefore, studying these features is important for understanding the overall dynamics of turbulent boundary layers and the development of flow control strategies or near-wall flow modifications. However, compared to the extensive number of incompressible investigations much less is known about the structural characteristics for compressible turbulent boundary layer flows. Therefore, in this investigation turbulent boundary layers developing on a flat plate over a range of Reynolds numbers and Mach numbers are considered in order to investigate the effect of compressibility on coherent structures. More specifically, measurements are performed on a flat plate model in the Trisonic Wind Tunnel Munich (TWM) for $0.3 < \mathrm{Ma} < 3.0$ and a friction Reynolds number of $2700 < \mathrm{Re}_\tau < 14\,800$ or $19\,800 < \mathrm{Re}_{\delta_2} = \rho_e u_e \theta/\mu_\mathrm{w} < 40\,800$. Velocity fields are recorded using planar particle image velocimetry methods (PIV and stereo-PIV) in three perpendicular planes, i.e. streamwise-wall-normal (*xz*), spanwise-wall-normal (*yz*), and wall-parallel (*xy*). Using multi-point statistical methods it was found that the streamwise spatial extent of coherent structures in the log-law layer slightly increases with increasing Mach number. Furthermore, a distinct increase in the spanwise spacing of these structures was found for the supersonic cases when compared to the subsonic and transonic turbulent boundary layers.

Introduction

The coherent structures present in zero pressure gradient (ZPG) turbulent boundary layers has been studied extensively in the past decades and many statistical and structural properties of the flow are well known, as documented in the extensive review by Wallace (2012). High- and low-momentum large-scale coherent motions residing in the log-law layer called superstructures have been of particular focus in the last two decades, Adrian *et al.* (2000); Ganapathisubramani *et al.* (2005); Hutchins & Marusic (2007); Monty *et al.* (2009); Buchmann *et al.* (2016). A fascinating property of the superstructures is their streamwise length which is on average about $6\delta - 8\delta$. However, instantaneously they can extend up to $10\delta - 20\delta$ in the streamwise direction. In addition, they strongly meander in the spanwise direction (Hutchins *et al.*, 2011) and it has been shown that they can carry a relatively large a portion of the layer's turbulent kinetic energy, especially at large Reynolds numbers. In effect, they contribute mainly to the second peak in the streamwise velocity fluctuations forming at high Reynolds numbers (Fernholz & Finley, 1996; Monty *et al.*, 2009; Samie *et al.*, 2018). Therefore, the investigation of these superstructures is important for understanding the overall dynamics of turbulent boundary layers. However, compressibility effects on the coherent structures is by far less studied, mostly due to the many technical challenges these types of flow present.

For compressible turbulent boundary layers, one of the first direct comparisons of compressible boundary layers was done by Smits *et al.* (1989) using the correlated signals from a traversed hotwire for M = 0.1 and 2.9. They concluded that the spanwise spacing of structures remains the same for subsonic and supersonic, but the streamwise scales of the mass flux $(\rho u)'$ are twice as big for the subsonic case when compared to the supersonic case. A survey done by Smits & Dussauge (2006) of available supersonic measurements, mostly from using hot-wire, concluded that for increasing Mach number and Reynolds number the streamwise length scales decrease significantly while the spanwise scales remain unaffected by both Reynolds number and Mach number.

More recently investigations using particle image velocimetry (PIV) techniques to characterize the structural properties of supersonic boundary layers include Ganapathisubramani *et al.* (2006) where they show coherent structures in a turbulent boundary layer at Mach 2 at $\mathrm{Re}_\theta = 35\,000$ ($\mathrm{Re}_\tau = 5600$) with planar PIV in streamwise-spanwise planes (wall parallel) and observe an underlying similarity to incompressible case. Using two-point correlations of velocity fluctuations, Ganapathisubramani *et al.* (2006) showed that the streamwise lengths scales for a Mach 2 turbulent boundary layer were as much as 4 times larger than an incompressible case while the spanwise spacing remains similar to the incompressible case. The increase in streamwise length scales with Mach number is in contrast to the survey of hot-wire measurements provided in Smits & Dussauge (2006), however they attribute this to a Reynolds number effect or the difference between $(\rho u)'$ and u' correlations. Furthermore, direct numerical simulations of a Ma = 2 turbulent boundary layer at $\mathrm{Re}_\tau = 1120$ or $\mathrm{Re}_{\delta_2} = 3900$ show that the streamwise velocity length scales do not change when compared to the incompressible case, while the spanwise wavelengths are slightly larger for the computed supersonic flow when compared to experimental incompressible data, Pirozzoli & Bernardini (2011). Other experimental investigations of compressible boundary layers include Elsinga *et al.* (2010) a tomographic-PIV investigation of coherent structures in the Mach 2 turbulent boundary layer at $\mathrm{Re}_\theta = 34\,000$ and found that packages of elongated structures appear. More recently Buchmann *et al.* (2016) investigated large scale motions up to Ma = 0.8 and their interaction with the near wall pressure signal.

As the past experiments performed in different facilities do not lead to consistent results. The motivation for the

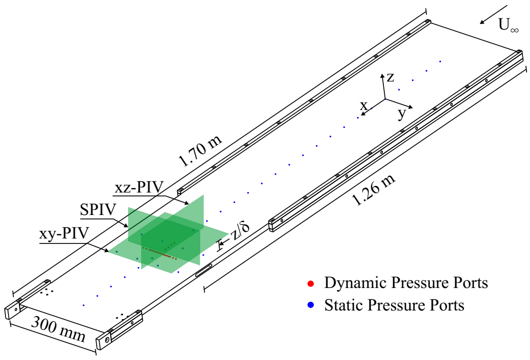

Figure 1: Flat plate boundary layer model used in Trisonic Wind Tunnel Munich (TWM). Planar PIV measurement planes location and orientation are indicated and labeled. Coordinates (x, y, z) correspond to streamwise, spanwise and wall-normal directions respectively.

current study is to investigate experimentally the structural topology of large scale structures at subsonic, transonic, and supersonic Mach numbers in the same test facility by means of state-of-art PIV techniques. The analysis consider the characteristic streamwise and spanwise scales of super-structures in the log-law layer over a Mach number range $0.3 < \mathrm{Ma} < 3.0$.

1 Experimental Systems and Methods

The Trisonic Wind Tunnel Munich (TWM) is a blow-down type wind tunnel with a 300 mm × 675 mm (width × height) test section. A two-throat system consisting of an adjustable Laval nozzle and an adjustable diffuser allows for a stable operating Mach number range from 0.2 to 3.0. The stagnation pressure is controlled by a pressure regulation valve and is adjustable between $p_0 = 1.2\,\mathrm{bar}$ and $5.0\,\mathrm{bar}$. This allows to set the Reynolds number independently of the Mach number. The corresponding Reynolds number range is $(4-78)\times 10^6\,\mathrm{m}^{-1}$. The stagnation pressure p_0 and temperature T_0 are recorded by two sensors in the settling chamber. The facility has two holding tanks that can be pressurized up to 20 bar above ambient pressure, with each tank holding a volume of 178 m^3 of air. This amount of air is sufficient for run times in the order of 100 seconds for the cases discussed below. The wind tunnel's test section is enclosed by a plenum chamber and also has the ability to apply boundary layer suction at both the vertical and the horizontal walls independently. A more detailed description of the freestream velocity and pressure fluctuations in the TWM can be found in Scharnowski *et al.* (2018).

A flat plate boundary layer model was mounted in the test section of the TWM for this investigation. A sketch of the model and coordinate system is shown in figure 1. The overall length of the model in the streamwise direction is 1.70 m, resulting in a turbulent boundary layer thickness of 13 − 20 mm at the measurement location, 1.26 m downstream of the leading-edge. Furthermore, a resistance based temperature sensor was installed just under the top surface, via a milled out cavity on the bottom side, in order to estimate the wall temperature T_w.

The freestream fluid properties in the settling chamber and the test section are outlined in table 1. The fluid properties in the freestream are calculated using the isentropic expansion equations and are denoted with the subscript e, e.g. the edge temperature T_e. Since the temperature of wall is known and the static pressure at the edge is the same at the wall ($p_e = p_\mathrm{w}$), ρ_w can be calculated from the ideal gas law. The viscosity at the wall and the edge is estimated from the Sutherland Modell (Smits & Dussauge, 2006).

Table 1: Flow field properties.

Ma_e		0.3	0.8	2.0	3.0
p_0	[bar]	1.5	1.5	2.2	4.5
t_0	[K]	288	288	287	288
t_e	[K]	282	255	160	103
ρ_e	[kg/m^3]	1.74	1.34	0.614	0.415
μ_e	[N s/m^2]$\times 10^{-5}$	1.76	1.63	1.09	0.71
ν_e	[N^2/s]$\times 10^{-5}$	1.02	1.21	1.77	1.75
u_e	[m/s]	101	256	506	610
t_w	[K]	289	288	283	283
ρ_w	[kg/m^3]	1.70	1.19	0.346	0.150
μ_w	[N s/m^2]$\times 10^{-5}$	1.79	1.79	1.77	1.77
ν_w	[N^2/s]$\times 10^{-5}$	1.06	1.50	5.01	11.7

2 Mean Velocity Field

The mean streamwise velocity profile shown in figure 2 was calculated by transforming the u velocity component with the van-Driest transformation (van Driest, 1951), see equations (1) and (2). This transformation takes into account the temperature at the wall and the edge. For sub-hypersonic Mach numbers the transformation is sufficiently valid (Smits & Dussauge, 2006). Then the transformed velocity is fit to the standard logarithmic "Law-of the Wall" plus the Coles correction factor, see equation (3). The mean flow parameters are outlined in table 2. What is important to note is the Reynolds number, namely the classical incompressible wall-turbulent Reynolds number Re_τ becomes small for Ma = 2.0 and 3.0 despite having large u_τ. This is because the kinematic viscosity at the wall is large and therefore a more useful Reynolds number to compare incompressible and compressible is $\mathrm{Re}_{\delta_2} = \rho_e u_e \theta / \mu_\mathrm{w}$. The edge flow properties are calculated by assuming an isentropic expansion by the Laval nozzle. Since the static pressure at the edge is the same at the wall according to boundary layer theory and the wall temperature T_w is measured, the density at the wall can be calculated from the ideal gas law. The kinematic viscosity at the wall can then be calculated via the Sutherland-Modell (Smits & Dussauge, 2006).

$$u^* = \frac{u_e}{b} \sin^{-1}\left(\frac{2b^2(u/u_e) - a}{\sqrt{a^2 + 4b^2}}\right) \tag{1}$$

$$a = \left(1 + r\frac{\gamma - 1}{2} Ma_e^2\right)\frac{T_e}{T_\mathrm{w}} - 1; b = r\frac{\gamma - 1}{2} Ma_e^2 \frac{T_e}{T_\mathrm{w}} \tag{2}$$

$$u_{vd}^+ = \frac{u^*}{u_\tau} = \frac{1}{\kappa}\log\left(\frac{u_\tau z}{\nu_\mathrm{w}}\right) + C^* + \frac{2\Pi}{\kappa}\sin^2\left(\frac{\pi}{2}\frac{z}{\delta_c}\right) \tag{3}$$

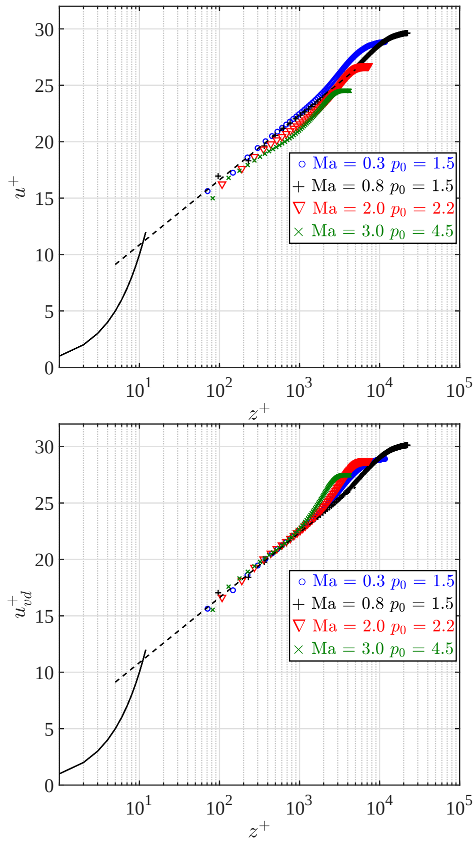

Figure 2: Inner scaled mean velocity profile for (top) u^+ and (bottom) Van-Driest transformed u^+_{vd} for 0.3 < Ma < 3.0.

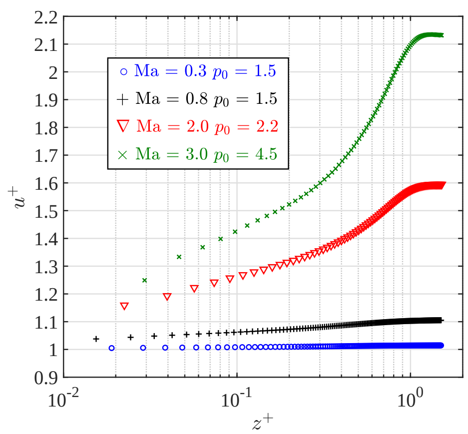

Figure 3: Mean density $\bar{\rho}$ normalized with fluid density at the wall ρ_w profile in the wall normal (z) direction.

3 Structural Analysis

In this section the structural properties of the turbulent boundary layers will be analyzed using multi-point correlations and spatial spectral methods.

3.1 Streamwise Characteristics

To give an overview of the turbulent boundary layer characteristics the streamwise development of the turbulent boundary layer in the streamwise-wall-normal (xz-plane) is considered in this section, see figure 4 for an exemplary instantaneous velocity field at Ma = 0.3. The long streamwise

Table 2: Boundary layer parameters.

Ma_e		0.3	0.8	2.0	3.0
δ_{99}	[mm]	24.5	26.9	14.0	14.1
Π	[-]	0.28	0.19	0.47	0.55
u_τ	[m/s]	3.41	8.42	18.3	23.8
Re_τ	[-]	7785	14 888	4807	2790
Re_θ	[-]	19 679	43 684	41 564	60 297
Re_{δ_2}	[-]	19 886	40 803	26 275	24 916

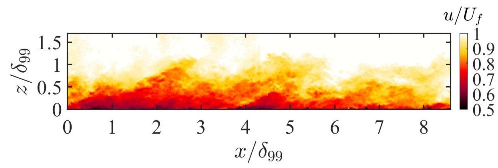

Figure 4: Instantaneous velocity field u/U_f where U_f = $0.99U_\infty$ at Ma = 0.3.

extent of the measurement plane is achieved by stitching together two overlapping camera images.

To determine the streamwise correlation of streamwise velocity fluctuations, u', a two point spatial correlation calculation is performed. Plotted in figure 5 are contours of R_{uu} at $z = 0.2\delta_{99}$, where $\xi_x = x_o + \Delta x$ and x_0 corresponds to the center of the field of view in the streamwise direction. Overlaid on the color contours is a straight line through the center of the correlations with an inclination angle of 14°. In both cases for the subsonic and supersonic boundary layers the typical inclination angle of the correlated velocity fluctuations is close to 14°. This is consistent with the inclination angle of the large-scale motions which is widely reported for incompressible ZPG flows, between 12° − 16° (Baars *et al.*, 2017; Adrian *et al.*, 2000; Marusic & Heuer, 2007). Investigations in compressible flows vary in the their results. Rayleigh scattering visualization measurements from Smith & Smits (1995) estimate between 30° − 60° inclination angle at Ma = 2.5. Correlations of u' from PIV measurements of at Ma = 0.8 and 3.0 turbulent boundary layers report inclination angles of 12° − 13° (Buchmann *et al.*, 2014) and 17° − 20° (Ringuette *et al.*, 2008).

The streamwise extent of the R_{uu} appears slightly longer for the supersonic case in comparison to Ma = 0.3. However, due to low-level correlation below 0.2 with the surrounding field for Ma = 0.3, conclusions about the spatial extent of these low correlation values must be done with caution. This low-level correlation is likely related to the nominal freestream turbulence intensity level in this blowdown wind tunnel (Scharnowski *et al.*, 2018). Nevertheless, the contour lines corresponding to R_{uu} = 0.2 appear slightly larger in the streamwise direction. To confirm this, the spatial spectral density was calculated for Ma = 0.3 and 2.0 and is plotted in figure 6. In these plots the highest value contour level of the normalized pre-multiplied velocity spectra, $(\bar{\rho}/\rho_w)k_x\Phi_{uu}/u_\tau^2$, appears at a streamwise wave length of $\lambda_x/\delta_{99} \approx$ 2.5 and 3.5 for Mach 0.3 and 2.0 respectively. While measurements closer to the wall were not possible in

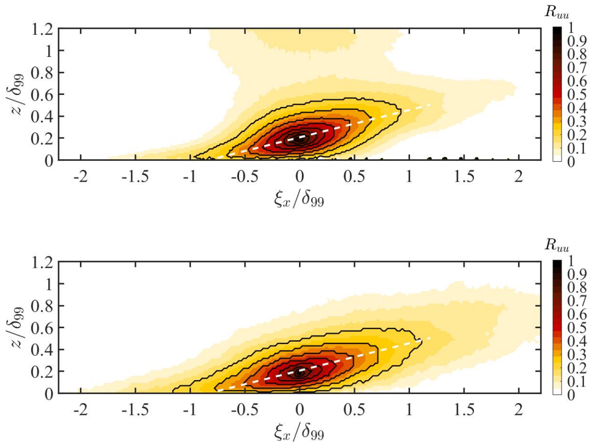

Figure 5: Two-point correlation R_{uu}, at $z = 0.2\delta_{99}$ for (top) Ma = 0.3 and (bottom) Ma = 2.0. Horizontal axis is $\xi_x = x_o + \Delta x$ where x_0 is the center of the field of view. Solid black contour lines range from 0.2 to 1 in 0.1 increments. White dashed line is plotted with 14° inclination angle.

these experiments, this peak in the spatial spectral plots is indicative of the secondary peak (Fernholz & Finley, 1996; Monty *et al.*, 2009; Samie *et al.*, 2018) in the streamwise velocity fluctuations. Since this peak is associated with the meandering superstructures in the log-law layer, it can be concluded that the superstructures are slightly more energetic for Ma = 2.0 as compared to 0.3 in the measurements presented herein even though the friction based Reynolds number is larger for Ma = 0.3 (Re_τ = 7785) than Ma = 2.0 (Re_τ = 4807), demonstrating that Re_τ is not a good reference value for comparing compressible and incompressible boundary layers.

3.2 Cross-Flow Structures

In order to visualize and analyze the organization of coherent flow structure in the spanwise direction at different wall normal heights, a stereo PIV measurement was performed in a cross-stream plane for all Mach numbers, see figure 7 for an exemplary instantaneous velocity field. In this section, the characteristic spatial distribution of coherent structures in the spanwise direction via multi-point statistics and spatial spectral calculations are presented.

In order to compare the spanwise spacing of coherent structures as a function of Mach number, slices of the correlation R_{uu} at z/δ_{99} = 0.1 for Ma = 0.3, 0.8, 2.0, and 3.0 are plotted in 8. In this figure, the spanwise (y-direction) shift is represented as ξ_y, where $\xi_y = y_o + \Delta y$ and y_0 is the center of the field of view in the spanwise direction. For all Mach numbers, there is a central positive correlation peak flanked on either side by a smaller negative correlation. However, the spacing between the negative correlation peaks is distinctly different for Ma = 0.3 and 0.8 when compared to the supersonic cases at Ma = 2.0 and 3.0. For the subsonic cases the spacing between the negative correlations is $0.6\delta_{99}$ compared to the a spacing closer to δ_{99} for the supersonic cases.

To confirm this finding at different wall normal distances, the spectra of the streamwise velocity pre-multiplied with the spanwise wave number as a function of spanwise wave lengths and wall normal distance for Ma = 0.3 and Ma = 2.0 are plotted in figure 9. According to these plots the most energetic spanwise wavelengths for the subsonic case are less than λ_y/δ_{99} and generally remain below that value for increasing wall normal distance. Contrary to this, the most energetic wavelengths in the log-law region of the supersonic case are slightly above λ_y/δ_{99}, which is consistent with the findings in figure 8. This demonstrates, that the effect of Mach number is to increase the spanwise spacing of the coherent structures.

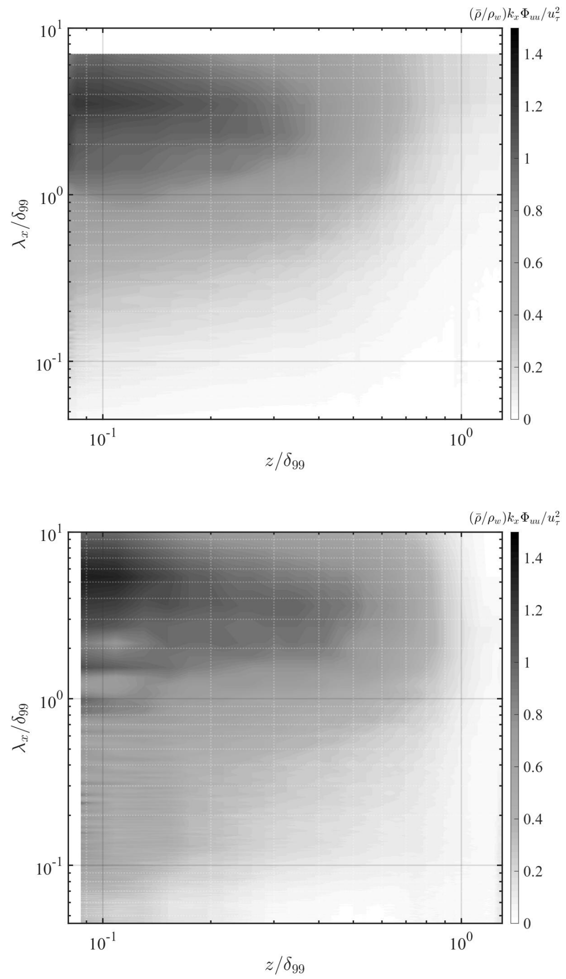

Figure 6: Pre-multiplied streamwise direction spectral density for (top) Ma = 0.3 and (bottom) Ma = 2.0 cases.

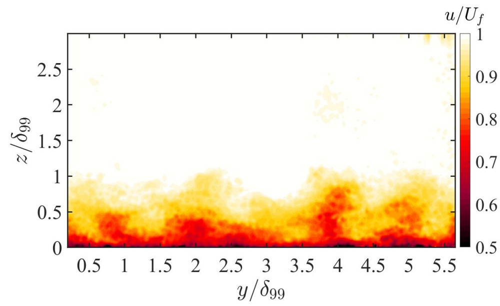

Figure 7: Instantaneous cross-stream velocity field at Ma = 2.0.

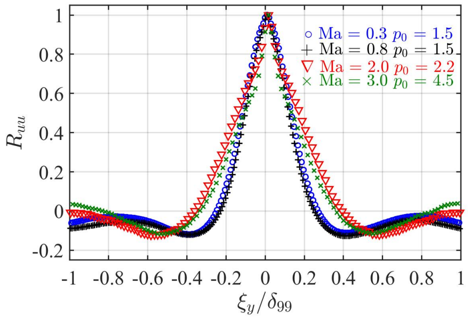

Figure 8: Spanwise distribution of R_{uu} for Ma = 0.3, 0.8, 2.0, and 3.0 at $z/\delta_{99} = 0.1$. On the horizontal axis $\xi_y = y_0 + \Delta y$ where y_0 is the center of the field of view in the spanwise direction.

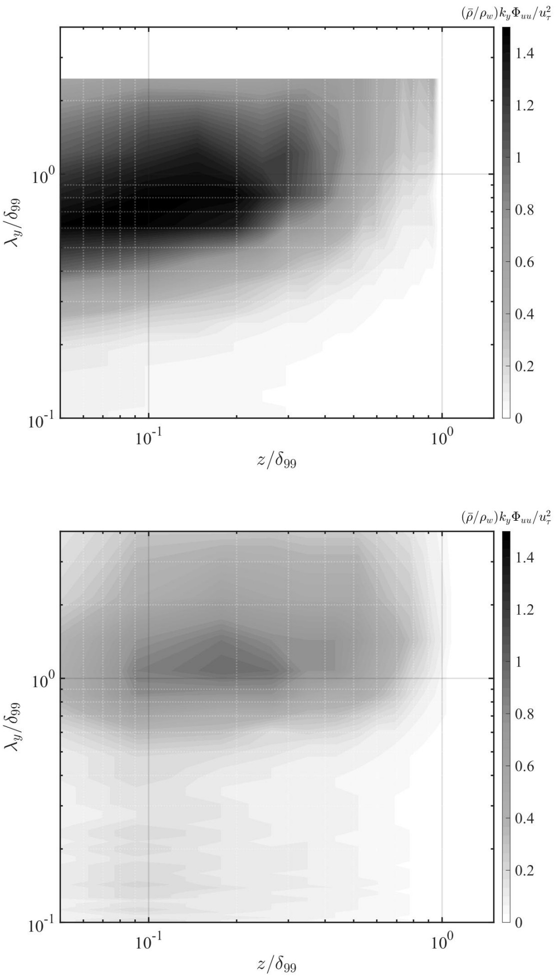

Figure 9: Pre-multiplied spanwise spectral density for (top) Ma = 0.3 and (bottom) Ma = 2.0 cases.

3.3 Elongated Structures in Wall Parallel Plane

To confirm that long high- and low-momentum meandering superstructures exist in the log-law region over the range of Mach numbers investigated, PIV measurements in a wall-parallel plane (xy) were performed. Two exemplary instantaneous fields in this plane are provided in figure 10 for Ma = 0.3 and 3.0. What is immediately evident

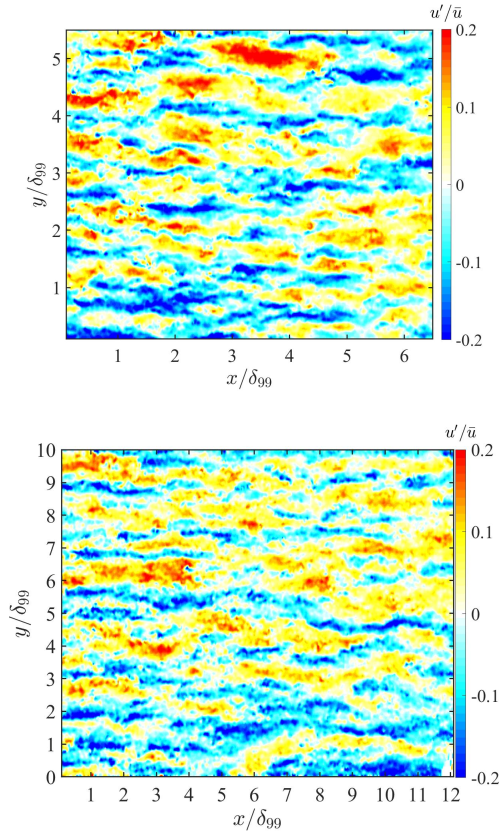

Figure 10: Instantaneous streamwise velocity fluctuation fields in the xy plane for (top) Ma = 0.3 and (bottom) Ma = 2.0. Measurement plane location at z/δ_{99} = 0.1 and 0.2 for Ma = 0.3 and 2.0 respectively.

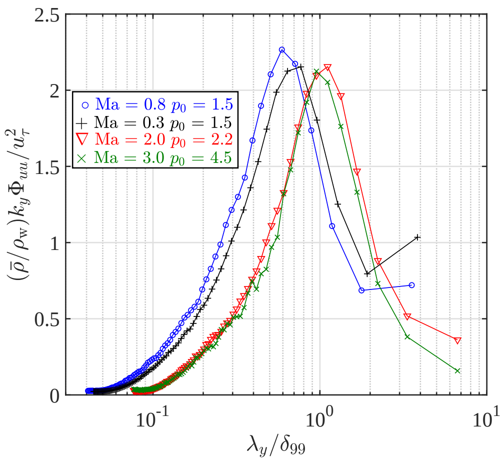

Figure 11: Pre-multiplied spanwise direction spectral density for 0.3 < Ma < 3.0.

in these figures is the meandering streaky structure in both subsonic and supersonic cases, confirming the existence of superstructures in both flows. Clearly, the large scale structures or superstructures are present in both cases and have a streamwise extent of several δ_{99} and a spanwise spacing of around δ_{99}.

To further investigate the spacing the in the spanwise direction and confirm the result from the previous section where it was demonstrated that the spanwise spacing of structures was larger for the supersonic case in comparison to the subsonic case, the spectral density of the streamwise velocity fluctuations in the spanwise direction was calculated and plotted in 11. In this plot the location of the peak in the energy spectra is location just below $\lambda_y/\delta_{99} = 1$ for both subsonic cases and slightly larger than $\lambda_y/\delta_{99} = 1$ for the supersonic cases. While the location of the wall-parallel measurement plane was at slightly different z/δ_{99} for the subsonic and supersonic cases due to the changing boundary layer thickness, the finding that the structure spacing is larger for supersonic as compared to subsonic is consistent with the finding in the previous section.

4 Concluding Remarks

In this work, turbulent boundary layers developing on a flat plate over a range of $0.3 < \mathrm{Ma} < 3.0$. are measured with planar 2D and stereo-PIV. It is important to note that the comparison of subsonic, transonic, and supersonic turbulent boundary layers is done in the same wind tunnel facility, were the flow quality is well documented for the range of Mach numbers considered, Scharnowski *et al.* (2018).

It was demonstrated in this work that the van Driest scaling of the mean velocity profile produced a good collapse of profiles over the range of Mach numbers investigated. Furthermore, it was shown that the friction based Reynolds number, which is commonly used to characterize incompressible wall bounded turbulence, is not as useful for compressible turbulence due to the large viscosity found near the wall which leads to relatively small friction based Reynolds numbers despite extremely large u_τ.

Furthermore, multi-point statistical and spatial spectral methods were used to determine the spacing and spatial extent of large scale features in the streamwise and spanwise directions. It was shown that large scale coherent motions exist in supersonic boundary layers qualitatively similar to the incompressible cases found in literature. However, the length of the streamwise energetic wavelengths associated with superstructures was shown to increase slightly for the supersonic cases as compared to the subsonic Mach numbers. Which is in contrast to decrease in streamwise mass flux correlation with increase Mach number shown in Smith & Smits (1995). Furthermore, while a slight increase in the streamwise correlation with increasing Mach number was shown herein, it was not as large of an increase (4 times) as observed in Ganapathisubramani *et al.* (2006).

Finally, a distinct increase in the spanwise spacing of large-scale structures in the supersonic cases as compared to the Ma = 0.3 and 0.8 cases was demonstrated. In addition, it was also noticed that the spanwise spacing slightly increased with increasing Mach number, albeit only around 15%, in the DNS results of Pirozzoli & Bernardini (2011). However, experimental investigations, either hotwire or PIV, have not reported a variation in the spanwise spacing with Mach number.

This work is supported by the Priority Programme SPP 1881 Turbulent Superstructures funded by the Deutsche Forschungsgemeinschaft project number KA1808/21-1.

REFERENCES

Adrian, R. J., Meinhart, C. D. & Tomkins, C. D. 2000 Vortex organization in the outer region of the turbulent boundary layer. *J. Fluid Mech* **422**, 1–54.

Baars, W. J., Hutchins, N. & Marusic, I. 2017 Reynolds number trend of hierarchies and scale interactions in turbulent boundary layers. *Phil. Trans. R. Soc. A* **375** (2089).

Buchmann, N. A., Cierpka, C., Knopp, T., Schanze, D., Schröder, A., Hain, R. & Kähler, C. J. 2014 Large Scale Adverse Pressure Gradient Turbulent Boundary Layer Investigation by means of PIV and PTV. In *17th Inter. Symp. on the App. of Laser and Imaging Tech. to Fluid Mech., July 7-10, Lisbon, Portugal*.

Buchmann, N. A., Kücükosman, Y. C., Ehrenfried, K. & Kähler, C. J. 2016 Wall pressure signature in compressible turbulent boundary layers. In *Progress in Wall Turbulence 2*, pp. 93–102. Springer International Publishing.

van Driest, E. R. 1951 Turbulent boundary layer in compressible fluids. *J. Aero. Sci.* **18**, 145–160.

Elsinga, G. E., Adrian, R. J., van Oudheusden, B. W. & Scarano, F. 2010 Three-dimensional vortex organization in a high-reynolds-number supersonic turbulent boundary layer. *J. Fluid Mech.* **644**, 35–60.

Fernholz, H. H. & Finley, P. J. 1996 The incompressible zero-pressure-gradient turbulent boundary layer: An assessment of the data. *Progress in Aerospace Sciences* **32** (4), 245–311.

Ganapathisubramani, B., Clemens, N. T. & Dolling, D. S. 2006 Large-scale motions in a supersonic turbulent boundary layer. *J. Fluid Mech.* **556**, 271–282.

Ganapathisubramani, B., Hutchins, N., Hambleton, W. T., Longmire, E. K. & Marusic, I. 2005 Investigation of large-scale coherence in a turbulent boundary layer using two-point correlations. *J. Fluid Mech.* **524**, 57–80.

Hutchins, N. & Marusic, I. 2007 Evidence of very long meandering features in the logarithmic region of turbulent boundary layers. *J. Fluid Mech.* **579**, 1–29.

Hutchins, N., Monty, J. P., Ganapathisubramani, B., NG, H. C. H. & Marusic, I. 2011 Three-dimensional conditional structure of a high-reynolds-number turbulent boundary layer. *J. Fluid Mech.* **673**, 255–285.

Marusic, I. & Heuer, W. D. C. 2007 Reynolds number invariance of the structure inclination angle in wall turbulence. *Phys. Rev. Lett.* **99**, 114504.

Monty, J. P., Hutchins, N., NG, H. C. H., Marusic, I. & Chong, M. S. 2009 A comparison of turbulent pipe, channel and boundary layer flows. *J. Fluid Mech.* **632**, 431–442.

Pirozzoli, S. & Bernardini, M. 2011 Turbulence in supersonic boundary layers at moderate reynolds number. *J. Fluid Mech.* **688**, 120–168.

Ringuette, M. J., Wu, M. & Martín, M. P. 2008 Coherent structures in direct numerical simulation of turbulent boundary layers at mach 3. *J. Fluid Mech.* **594**, 59–69.

Samie, M., Marusic, I., Hutchins, N., Fu, M. K., Fan, Y., Hultmark, M. & Smits, A. J. 2018 Fully resolved measurements of turbulent boundary layer flows up to $Re_\tau = 20000$. *J. Fluid Mech.* **851**, 391–415.

Scharnowski, S., Bross, M. & Kähler, C. J. 2018 Accurate turbulence level estimations using PIV/PTV. *Exp. Fluids* **60** (1), 1.

Smith, M. W. & Smits, A. J. 1995 Visualization of the structure of supersonic turbulent boundary layers. *Exp. Fluids* **18** (4), 288–302.

Smits, A. J. & Dussauge, J. P. 2006 *Turbulent Shear Layers in Supersonic Flow*. Springer.

Smits, A. J., Spina, E. F., Alving, A. E., Smith, R. W., Fernando, E. M. & Donovan, J. F. 1989 A comparison of the turbulence structure of subsonic and supersonic boundary layers. *Phy. of Fluids A* **1** (11), 1865–1875.

Wallace, J. M. 2012 Highlights from 50 years of turbulent boundary layer research. *J. Turbulence* **13**, 1–70.